

# Initial Assessment of a Variable-Camber Continuous Trailing-Edge Flap System on a Rigid Wing for Drag Reduction in Subsonic Cruise

Corey Ippolito<sup>1</sup>, Nhan Nguyen<sup>2</sup>, Joe Totah<sup>3</sup>  
*NASA Ames Research Center, Moffett Field, CA 94035*

Khanh Trinh<sup>4</sup> and Eric Ting<sup>5</sup>  
*Stinger Ghaffarian Technologies, Inc., Moffett Field, CA 94035*

**In this paper, we describe an initial optimization study of a Variable-Camber Continuous Trailing-Edge Flap (VCCTEF) system. The VCCTEF provides a light-weight control system for aircraft with long flexible wings, providing efficient high-lift capability for takeoff and landing, and greater efficiency with reduced drag at cruising flight by considering the effects of aeroelastic wing deformations in the control law. The VCCTEF system is comprised of a large number of distributed and individually-actuatable control surfaces that are constrained in movement relative to neighboring surfaces, and are non-trivially coupled through structural aeroelastic dynamics. Minimization of drag results in a constrained, coupled, non-linear optimization over a high-dimension search space. In this paper, we describe the modeling, analysis, and optimization of the VCCTEF system control inputs for minimum drag in cruise. The purpose of this initial study is to quantify the expected benefits of the system concept. The scope of this analysis is limited to consideration of a rigid wing without structural flexibility in a steady-state cruise condition at various fuel weights. For analysis, we developed an optimization engine that couples geometric synthesis with vortex-lattice analysis to automate the optimization procedure. In this paper, we present and describe the VCCTEF system concept, optimization approach and tools, run-time performance, and results of the optimization at 20%, 50%, and 80% fuel load. This initial limited-scope study finds the VCCTEF system can potentially gain nearly 10% reduction in cruise drag, provides greater drag savings at lower operating weight, and efficiency is negatively impacted by the severity of relative constraints between control surfaces.**

## I. Introduction

Advanced light-weight materials show promise of increasing energy efficiency of modern aircraft in part through reduction of airframe weight. Lighter-weight wing structures constructed from these materials can provide sufficient load-carrying capacity for the aircraft with reduced structural rigidity. Increased structural flexibility may potentially degrade overall aerodynamic efficiency due to aeroelastic interactions between aerodynamic forces and wing-structure dynamics, which can have a significant impact on the aerodynamics of the aircraft. A recent NASA study<sup>1</sup> showed active control of wing aeroelasticity can be beneficial in achieving drag reduction. The study showed that highly flexible wing aerodynamic surfaces can be elastically shaped in-flight by active control of wing twist and vertical deflection in order to optimize the local angle of attack of wing sections to improve aerodynamic efficiency through drag reduction during cruise and enhanced lift performance during take-off and landing.

In this paper, we present an initial assessment of a new numerical model of a variable continuous trailing-edge flap (VCCTEF) system on a commercial transport-class fixed-wing aircraft in subsonic cruise. The VCCTEF system offers potential pay-off for drag reduction by active aeroelastic shape control<sup>2</sup>. This system employs light-weight

---

<sup>1</sup> Research Scientist, Intelligent Systems Division, corey.a.ippolito@nasa.gov, AIAA Member.

<sup>2</sup> Intelligent Systems Division, nhan.t.nguyen@nasa.gov, AIAA Associate Fellow.

<sup>3</sup> Intelligent Systems Division, joseph.j.totah@nasa.gov, AIAA Associate Fellow.

<sup>4</sup> Intelligent Systems Division, NASA Ames Research Center.

<sup>5</sup> Intelligent Systems Division, NASA Ames Research Center.

shape-memory alloy (SMA) technology for actuation and three separate chordwise segments shaped to provide a variable-camber to the flap. A VCCTEF conceptual schematic is shown in Figure 1 below. The VCCTEF system consists of 2-foot spanwise flap segments that can be individually actuated, resulting in the ability to control the wing twist as a function of span to improve the lift-to-drag ratio (L/D) at any aircraft gross weight or flight condition. This provides an advantage over conventional flap systems, since wing-twist is permanently set for one cruise configuration on conventional aircraft, and is typically set for 50% loading or mid-point on the gross weight schedule. The VCCTEF system offers the ability to set wing-twist for any gross weight and flight conditions. Wing-twist may be independently specified for climb, cruise and descent phases, achieving optimal L/D efficiency throughout all phases of flight. The individual 2-foot spanwise flap sections are connected with a flexible elastomeric covering with no gaps on the surface between flap segments, thus reducing drag by eliminating breaks in the flap continuity which otherwise would generate vorticity that results in a drag increase and also contributes to airframe noise<sup>2,3,4</sup>.

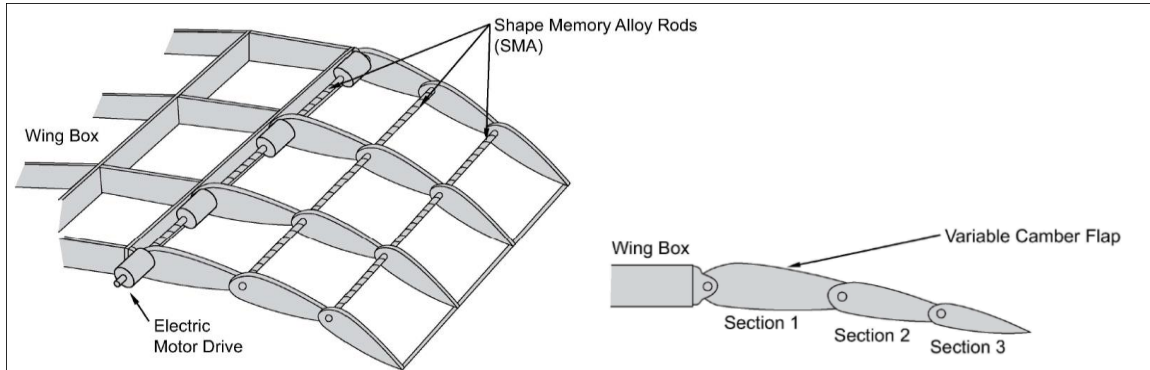


**Figure 1. VCCTEF Conceptual Schematic<sup>3</sup>.**

This paper presents an initial assessment of the drag-reduction potential for a VCCTEF system on a rigid wing without structural flexibility or aeroelastic interactions. Analysis is performed on a modified NASA Generic Transport Model (GTM) aircraft, which is based on a Boeing 757 airframe<sup>5</sup>. The GTM model was modified to incorporate a VCCTEF system consisting of 15 2-foot spanwise sections on each wing. Each segment contains three actuatable rotational joints. In this assessment we assume the deflection of each flap segment provides a third of the commanded angle to provide a smooth camber shape. Drag-reduction potential is calculated through direct numerical optimization of VCCTEF deflection angles on the modified GTM model to minimize drag at various fuel loads in cruise. The following study analyzes steady-state conditions only, assuming transient and unsteady aerodynamic effects can be neglected. Aerodynamic forces and moments are evaluated using the VORLAX software library<sup>5</sup>. VORLAX is a computational aerodynamic tool that utilizes vortex-lattice methods to evaluate the aerodynamics of arbitrary-shaped bodies. This tool utilizes potential flow technique to estimate induced drag in subsonic laminar flow regimes. The underlying assumptions in VORLAX are therefore extended to this analysis. This initial study was performed on a rigid aircraft assuming static wing geometry (e.g., invariant to aerodynamic loads). Aeroelastic effects and structural flexibility of the wing will be analyzed into follow-on studies based on models that were under development at the time of this initial study<sup>6</sup>.

## II. Model Description

The numerical analysis tool pipeline is shown conceptually in Figure 2 below. The model (detailed in <sup>8</sup>) is composed of three main components: a parametric geometry generator, the VORLAX aerodynamics evaluation, and a set of scripts that process the resulting aerodynamic data and determine the trim condition. The numerical optimization engine directly minimizes drag based on flap input utilizing numerical techniques.

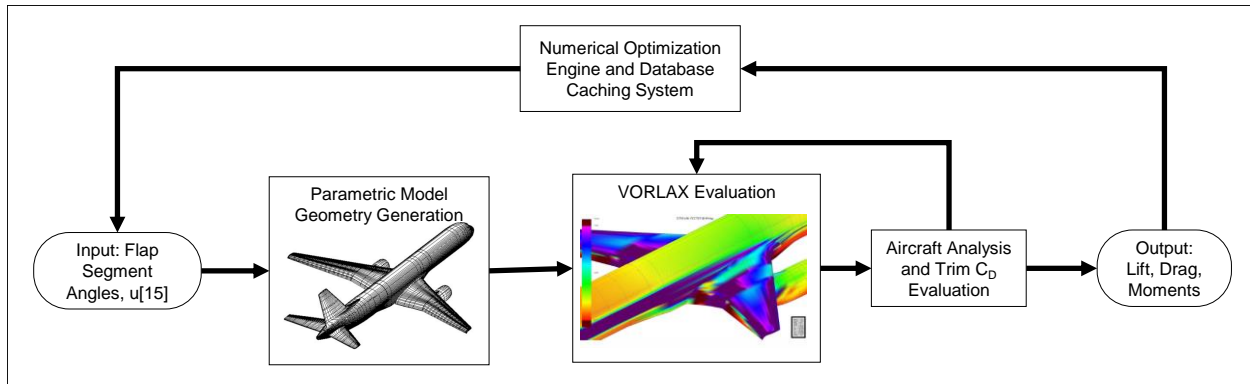


**Figure 2. Conceptual Processing Pipeline.** *This initial assessment was performed on the rigid-wing without aeroelastic considerations.*

The parametric geometry model shown in Figure 2 modifies the original NASA GTM geometric model with a 15-segment VCCTEF actuation system. The generated aircraft mesh has a total of 20,806 nodes and 19,908 quadrilateral elements. The configuration of the flaps is shown in Figure 3 below. Each 24-inch section has three camber flap segments that can be individually commanded. These camber flaps are joined to the next section by a flexible and supported material (shown in blue) installed with the same shape as the camber and thus providing continuous flaps throughout the wing span with no gaps in the resulting geometric mesh. The model parameters used in this study are given in Table 1 below.

**Table 1. Modified GTM+VCCTEF Model Parameters**

Empty Weight	150,000 lbs
Fuel Weight	50,000 lbs
Wing Reference Area	1951 ft <sup>2</sup>
Aspect Ratio	7.82
Mach Number	0.8
CL desired, 20% Fuel Load	0.2914
CL desired, 50% Fuel Load	0.3187
CL desired, 80% Fuel Load	0.3460
CL desired, 100% Fuel Load	0.3642
<i>VCCTEF System</i>	
Number of Control Surfaces	15 per wing
Maximum Deflection Angle	+/- 10 degrees
Maximum Allowed Relative Angle Constraint	3 cases studied: unconstrained, 1 degree, and 2 degrees between adjacent control surfaces

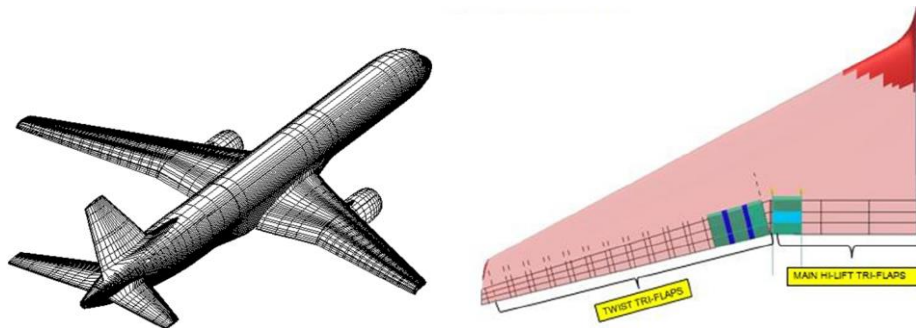


**Figure 3. Modified GTM Model (left), GTM Wing Configured with 15 VCCTEF Actuators<sup>6</sup> (right)**

The resulting geometric mesh is processed in the VORLAX engine over a range of angle of attacks, and the results are used to determine the trim state drag based on the given fuel load and total operating weight. The process for evaluation, given the input flap commands and fuel load, is summarized as follows.

1. Evaluate desired  $C_L$  as a function of fuel load and operating weight.
2. Generate the geometric mesh for the given flap deflection input vector  $u$  (assumes static/fixed geometry).
3. Evaluate  $C_L$  and  $C_D$  over a range of  $\alpha$ 's using VORLAX.
4. Fit a cubic hermite spline curve for interpolation of the  $C_L/C_D$  curve.
5. Interpolate to find  $C_D$  at the specified  $C_L(W)$ .

The  $C_L$  vs  $C_D$  curve for symmetric uniform flap deflections are shown in Figure 4. The minimum  $C_L/C_D$  point and trim  $C_L/C_D$  points given fuel loads of 20%, 50%, 80%, and 100% are highlighted. Uniformly adjusting the flap settings shifts the  $C_L/C_D$  curves and the resulting operating points as shown.

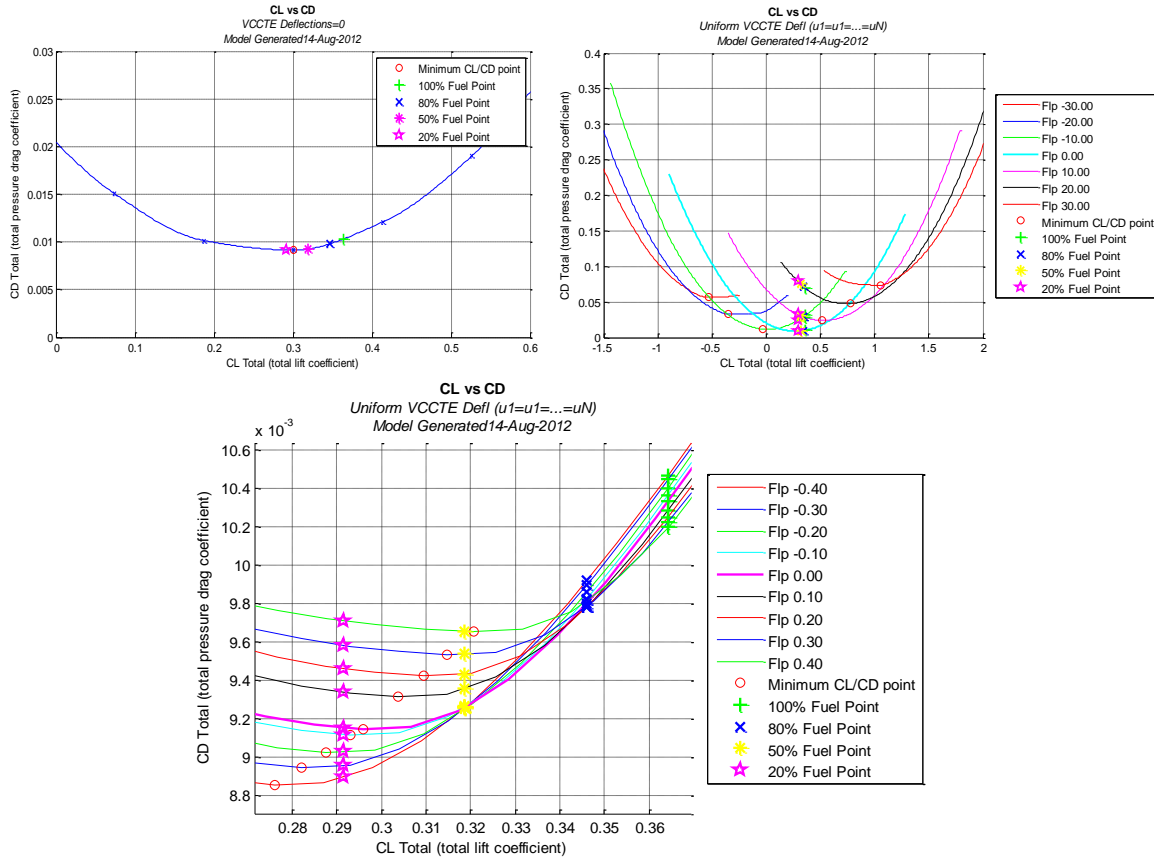


**Figure 4. VCCTEF Drag Polars.** Drag polar at zero deflection (top-left). Uniform symmetric flap deployment (top-right). Symmetric deployment over small flap angles (bottom).

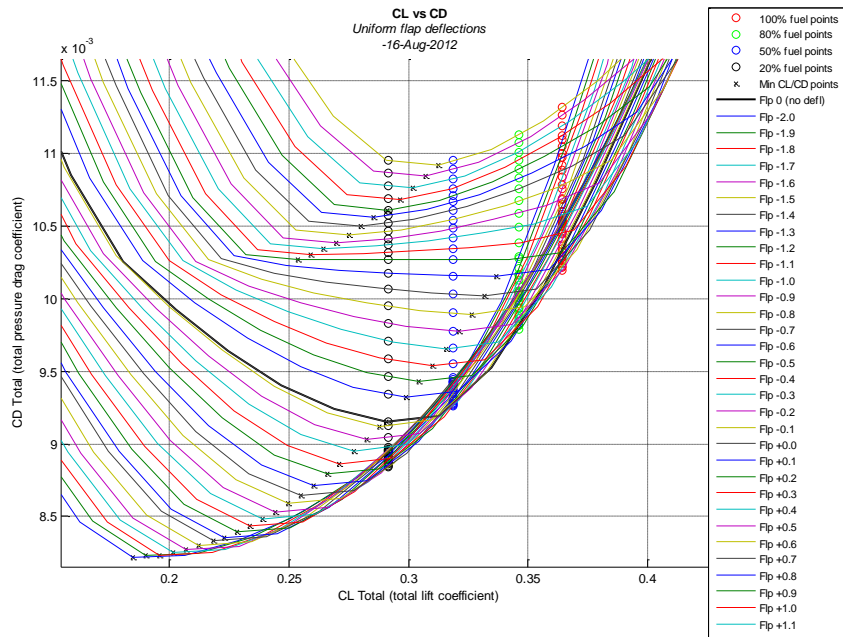


Figure 5. CL vs CD Effect of Small VCCTEF Deflections. Uniform symmetric flap deflection from -2.0 to +2.0 degrees.

### A. Effect of Uniform VCCTEF Deflections

The effect of symmetric uniform VCCTEF flap deflection on the total aircraft dynamics are shown in the following figures.

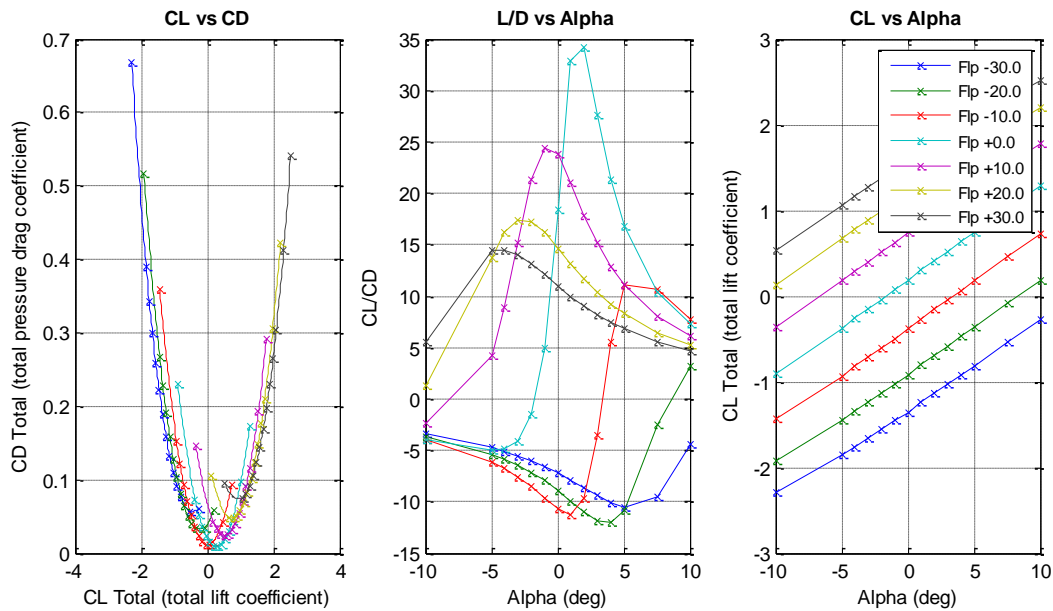
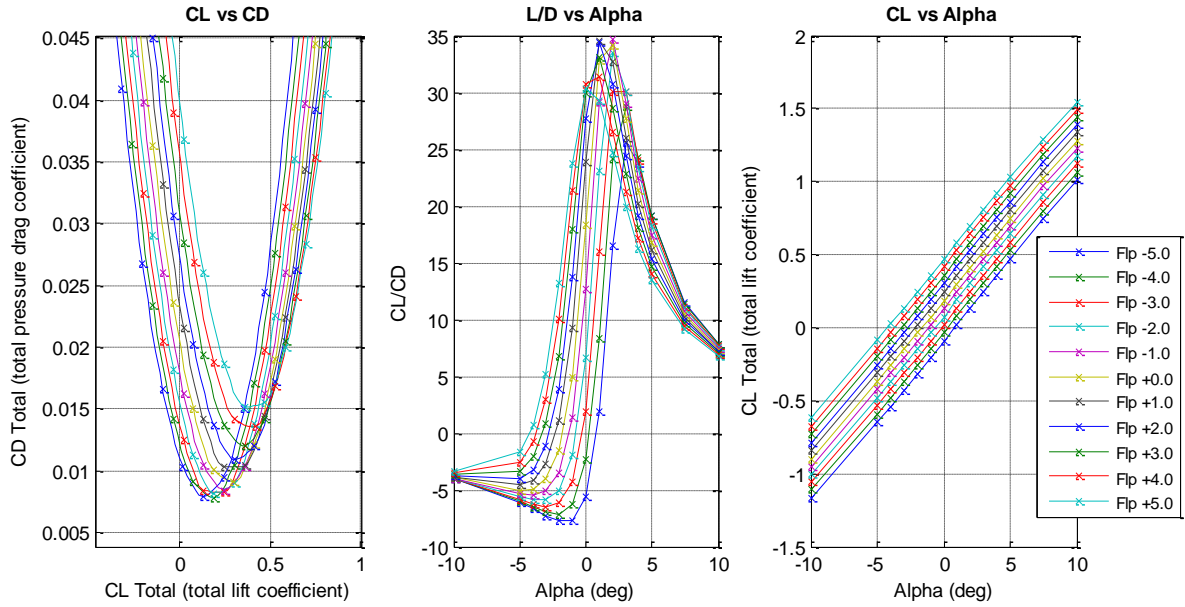
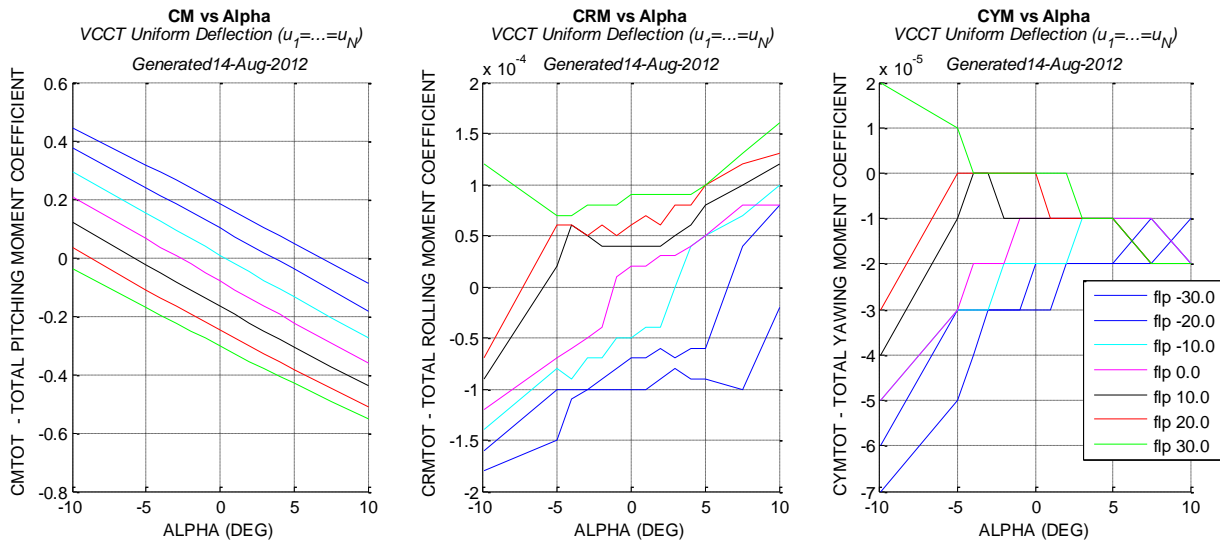


Figure 6. Effect of Uniform VCCTEF Deflection. CL vs CD, L/D, and CL-alpha plots shown for flap deflections from -30 to 30 with steps of 10 deg.



**Figure 7. CL vs CD, L/D, and CL.** Flap deflections from -5 to 5 with steps of 1 deg.



**Figure 8. Pitching, Rolling, and Yawing Moment Coefficients.** Coefficients plotted versus alpha for -30 to 30 deg. flap deflections. All VCCTE flaps are at the same deflection angle, with positive being trailing edge down.

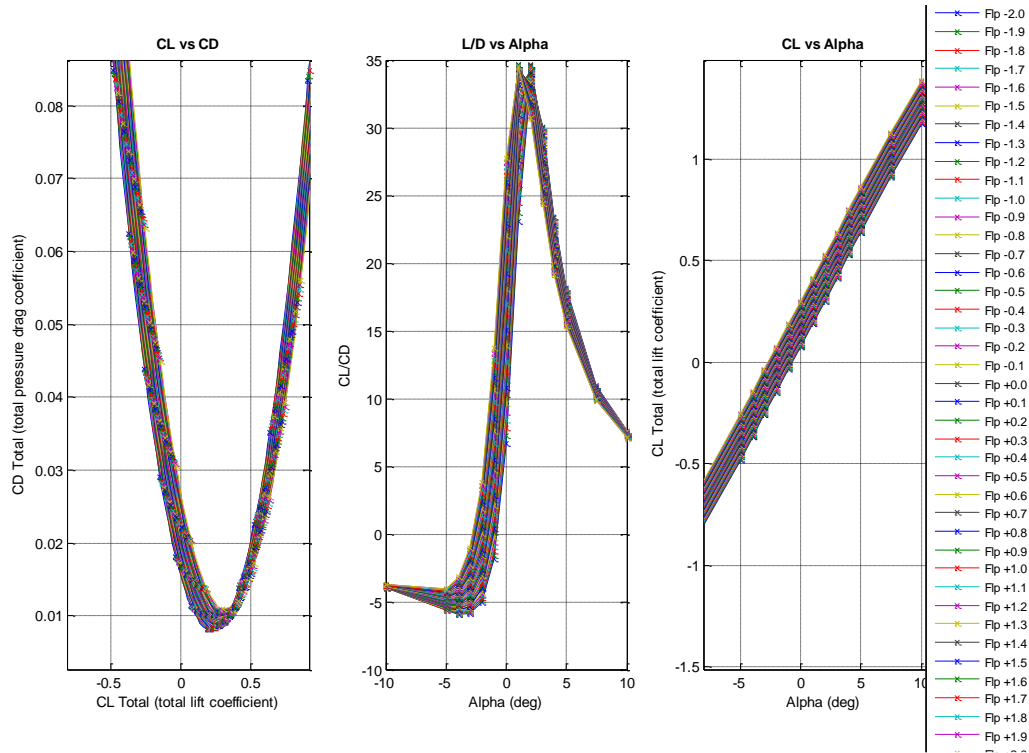


**Figure 9. Lift Drag Summary.** *Uniform deflections from -2.0 to +2.0 degrees.*

### B. Comparison of Parametric VCCTEF Model to Baseline GTM Model

The conversion of the baseline GTM geometry into a parametric model and replacing the conventional control surfaces with a smoothly varying VCCTEF geometry results in mesh variations between the original and resulting geometries. The differences between subsequent VORLAX analysis comparisons between the two models arise due to two sources: (1) model discrepancy errors introduced in the process of converting the static geometry to a parametric model, and (2) improved aerodynamic efficiency of VCCTEF geometry over fixed conventional control surfaces (eg, smooth contours blending the wing and control surface geometries, removal of gaps). The variations are highlighted in Figure 10 below. The drag polar shows decent correlation, but the parametric model results in a noticeable lift improvement, as seen in the shifted CL-alpha curve, and improved L/D efficiency at small angles of attack.

Unfortunately it is difficult to determine precisely what percentage of efficiency improvements shown in Figure 10 is due to the parametric conversion as opposed to model variations due to the parametric conversion process. Due to this difficulty, this assessment only compares drag improvements of a VCCTEF configuration against the undeformed parametric VCCTEF, rather than comparing against the original GTM geometry. Note that comparison against the original GTM would result in greater performance improvement.

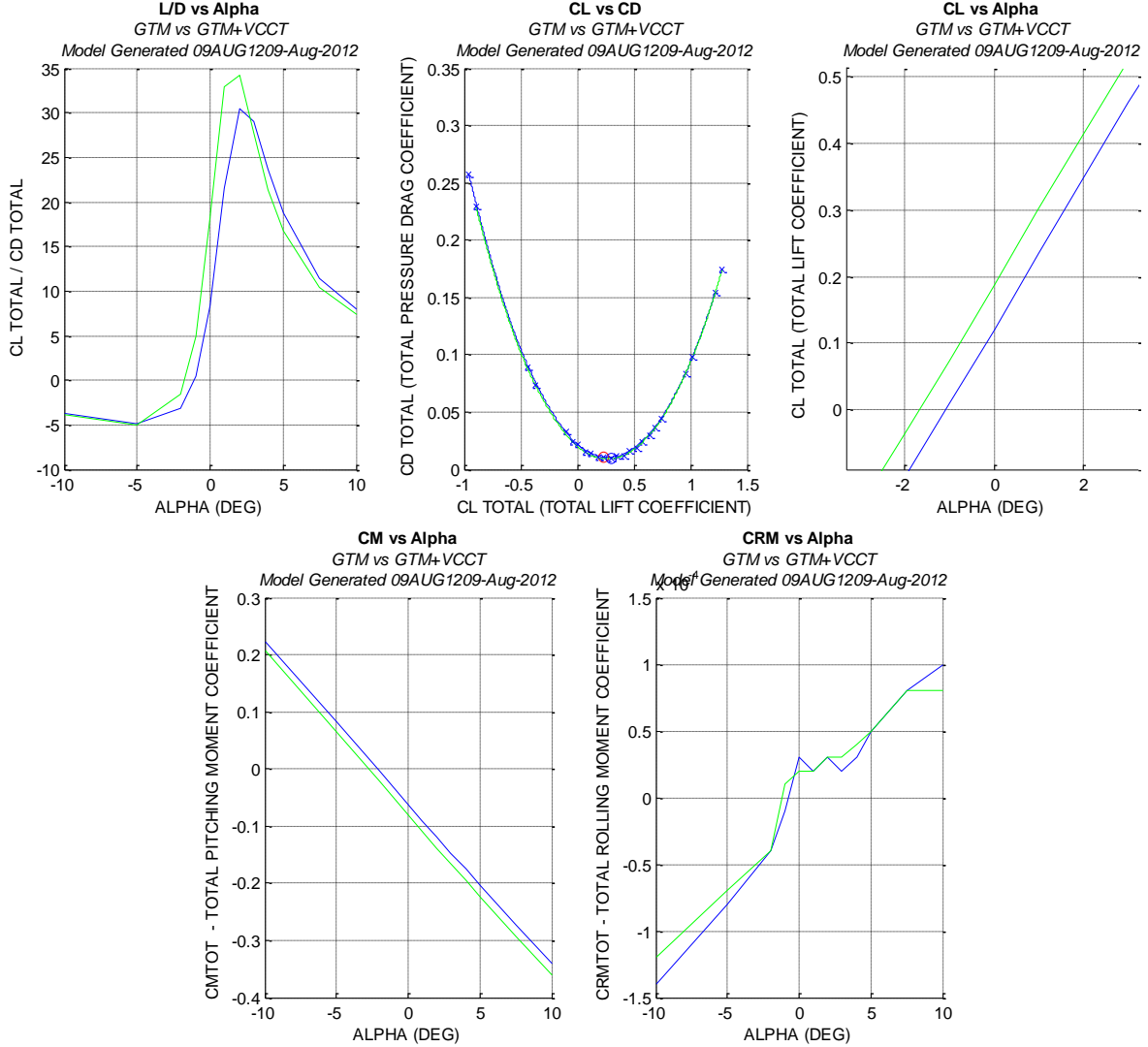


**Figure 10. Comparison of Parametric VCCTEF Model with Conventional GTM Model.** *Parametric model is shown in green, the original fixed geometry GTM model is shown in blue.*

### III. Optimization Study

#### C. Optimization Problem Statement

The drag minimization problem can be generally stated as follows. Find  $u^* = \arg \min_u (J(\mathbf{u}))$  subject to the following constraints

- C1.  $\|\mathbf{u}\|_\infty \leq u_{max}$
- C2.  $|u[j+1] - u[j]| \leq \Delta u_{max}$  for all  $j \in [1..M-1]$

where

$\mathbf{u} \in \mathbb{R}^{15}$  is the input vector of flap angle settings (degrees), and  $J(\mathbf{u}): \mathbb{R}^{15} \rightarrow \mathbb{R}$  is the optimization objective function.

For this study the objective function is given by

$$J(\mathbf{u}) = C_{D,trim}(\mathbf{u}, p_{fuel})$$

where  $p_{fuel}$  is the fuel load given in percent full (i.e., 0% when empty, 100% when carrying a full fuel load). The aircraft weight considered in this study is the sum of the fuel weight and empty weight ( $W_{empty}$ ). The lift coefficient,  $C_L$ , is thereby a function of  $p_{fuel}$  given by

$$C_L(p_{fuel}) = \frac{W_{empty} + p_{fuel} * W_{fuel}}{\frac{1}{2} \rho V^2 S}$$

where  $W_{fuel}$  is the weight of fuel at full capacity (i.e., when  $p_{fuel} = 100\%$ ). The assumption in this initial assessment is that aircraft geometry is uniquely determined by the input vector  $u$  at a given fuel load and is invariant to the resulting aerodynamic loads and aeroelastic deformation. The drag polar curve (CD versus CL) is determined by evaluating the aerodynamic forces and moments of the geometry over a range of attack angles. The CL versus CD curve is then interpolated to determine the trim  $C_D$  and alpha point, as illustrated previously in Figure 4.

#### D. Optimization Topology

Given a fixed geometry wing section, drag is expected to vary smoothly and convexly with flap deflection<sup>9</sup>, resulting in a unique trim alpha point with minimum drag. To verify the analytical tool results, a variational survey was conducted allowing 1 and 2 degrees of freedom. The variation of drag due to a single actuator is shown in Figure 11 below.

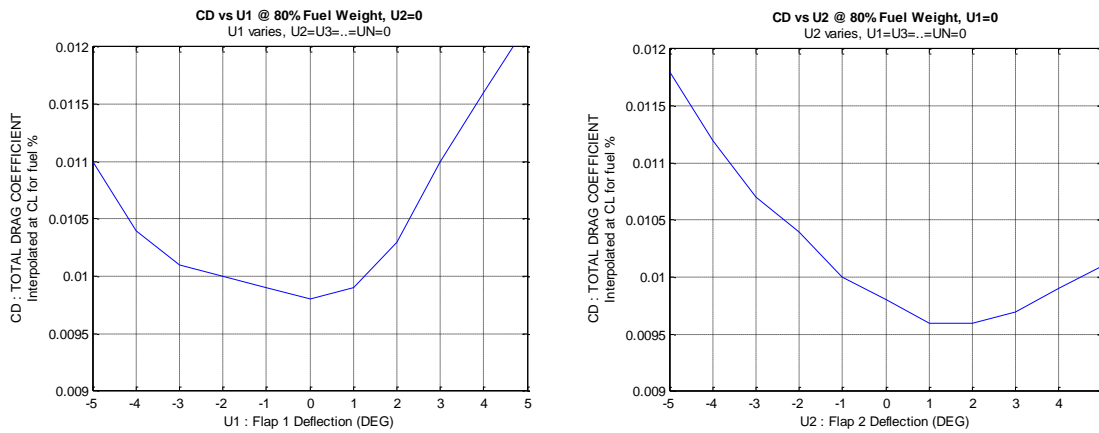


**Figure 11. Trim Drag Coefficient Versus Flap Deflection of a Single VCCTEF Control Surface.  $CD$  versus  $U1$  (left) and  $U2$  (right) shown for 80% fuel load case.**

The following plots show variation of the trim drag coefficient versus two control surfaces. Variation of  $U1$  and  $U2$  are shown, while the remaining control surfaces remain fixed. The optimization topology is largely convex, continuous, and differentiable. Variation of other inputs shows similar results, which matches theoretical expectations. Based on this observation, gradient-descent methods were chosen as the basis for the optimization approach.

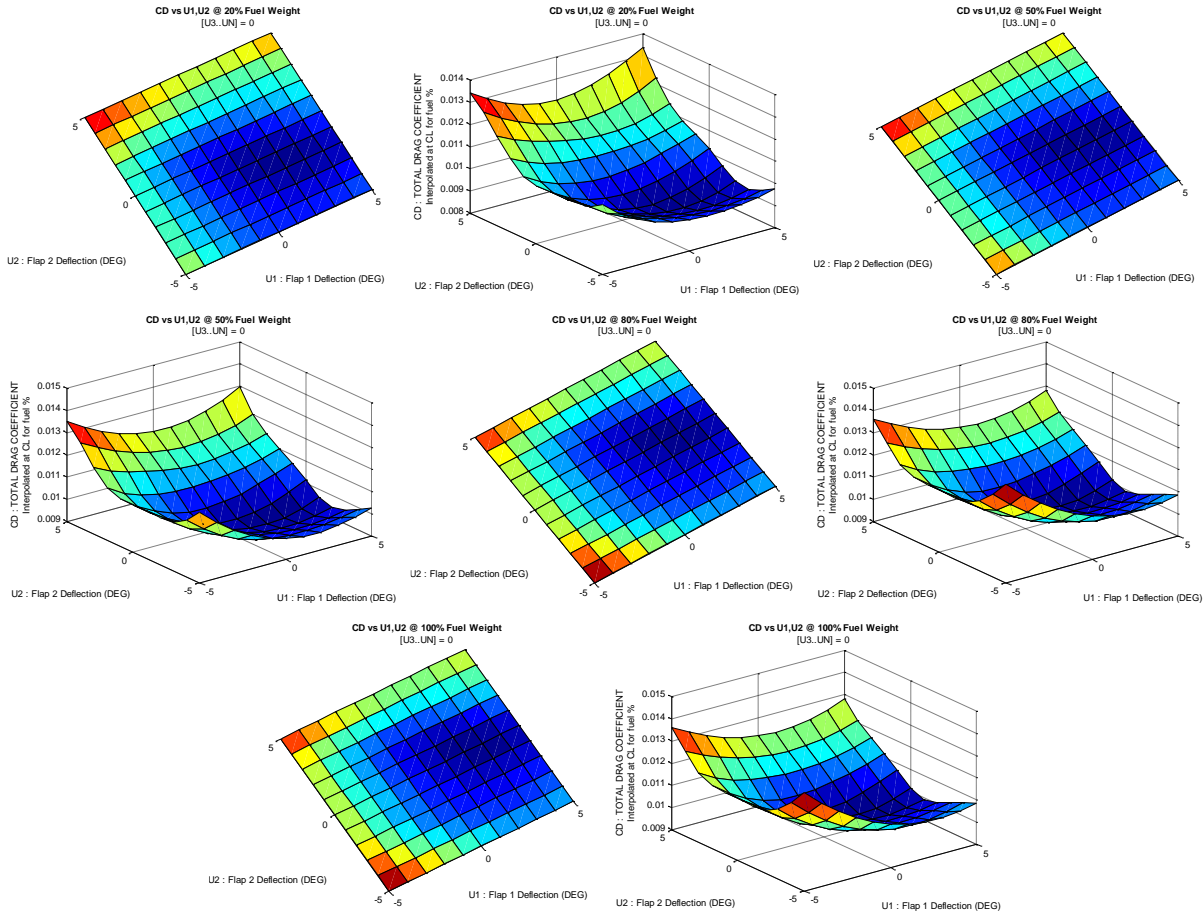


**Figure 12. Optimization Topologies for 2-DOF Case. Evaluated at fuel points of 20%, 50%, 80%, and 100%.**

### E. Effect of Constraints on 2-DOF Topology

The effect of applying constraints C1 and C2 are shown in the following diagrams. The constraint C1 is not expected to have an effect, as the optimal flap settings are not expected to be larger than the absolute deflection angles allowed. However, constraint C2 – which limits deflection angles between adjacent control surfaces – is expected to have a negative impact on the drag minimization potential for the VCCTEF system. As shown in the following figures, the minimum points may be located beyond the tolerance of C2, depending on the properties of the elastic material that is used to form a conformal surface between adjacent control surfaces. This study investigates 2-degree and 1-degree relative angle constraints. We note that if the optimal  $u$  point for the unconstrained minimization problem violates C1 or C2, we expect there will exist a unique optimal point on the constraint surface. In this case, we can search along the equality constraints for the optimal point.

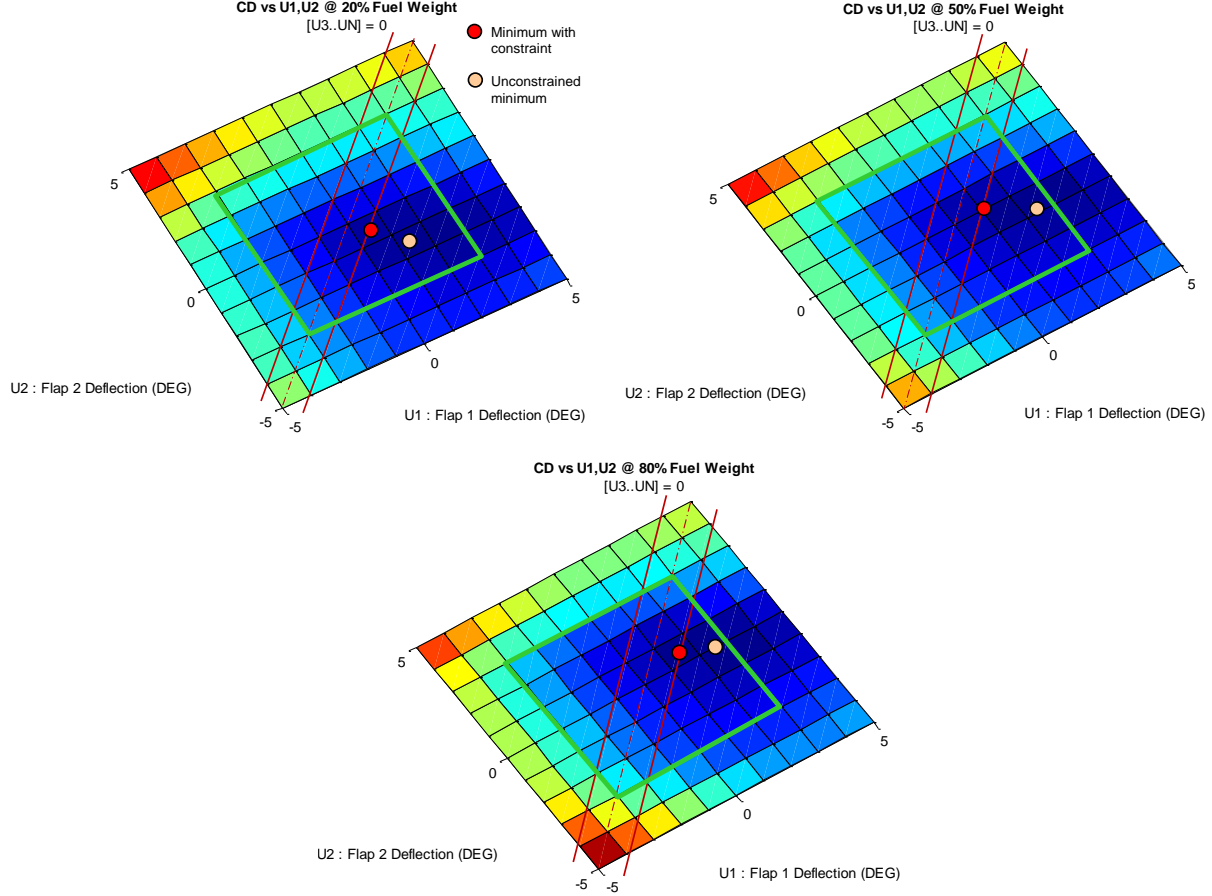


**Figure 13. Effect of Constraints C1 and C2 on Optimization.**

## F. Optimization Approach

In this initial assessment we perform direct numerical optimization of the model utilizing an iterative two-stage optimization scheme that involves a coarse then fine optimization technique.

### 1. Coarse Scheme

At a given  $u$ , let the gradient vector be given by

$$\nabla J(u) = \left[ \frac{\delta J}{\delta u_1}, \dots, \frac{\delta J}{\delta u_m} \right]$$

The gradient is estimated by a first-order derivative estimate

$$\frac{\delta J}{\delta u_i} \cong \frac{1}{\Delta u_g} [J(u_{i,j+}) - J(u_i)]$$

This requires  $M+1$  evaluations of  $J$ . Next, we create an affine parameterization along the gradient  $\nabla J(u)$  direction given by

$$\tilde{u}(k) = u_i - (k \cdot \Delta u_s \cdot \nabla J(u_i) \cdot \|\nabla J(u_i)\|_2^{-1})$$

Along this line we evaluate  $J$  an additional  $P$  times. The  $P+1$  samples are fit to a piecewise hermite cubic polynomial. The hermite curve is used to find the  $u$  which minimizes  $J(\tilde{u}(k))$  along the gradient direction. This algorithm will converge depending on properties of  $J$  (e.g.,  $J(u)$  is convex and  $\nabla J(u)$  is Lipschitz). The optimization algorithm details are shown below.

**Function  $u_{min} = OPTIMIZE (J, u_0, u_{max})$**

Problem

Find  $u_{min} = argmin_u J(u)$  subject to  $\|u\|_\infty \leq u_{max}$  and  $|u[j+1] - u[j]| \leq \Delta u_{max}$

Given

$u_0 \in \mathbb{R}^m$  Initial starting  $u$

$J(u): \mathcal{U} \rightarrow \mathbb{R}$  Objective function mapping

$u_{max}$  Max/min constraint on  $u$

Return

$u_{min} \in \mathbb{R}^m$  The optimal  $u$  found by the algorithm

Variables and Parameters

$i$  iteration counter

$k$  independent affine optimization parameter

$\Delta u_g$  delta  $u$  step for estimating the gradient

$\Delta u_s$  delta  $u$  step for affine interpolation and minimization

$\Delta ErrMin\%$  minimum error for termination of algorithm

1. hasConverged = false

2.  $i = 0$

3. While ! hasConverged

// Estimate the gradient  $\nabla J(u) = \left[ \frac{\delta J}{\delta u_1}, \dots, \frac{\delta J}{\delta u_m} \right]$

4.  $i++$

5. Evaluate  $J(u_i)$

6. For each actuator  $j = [1..M]$

7.  $u_{i,j+} = u_i + \delta_{(\Delta u_{g,j})}$  where  $\delta_{(\Delta u_{g,j})}[j' = j] = \Delta u_g \dots \text{and} \dots \delta_{(\Delta u_{g,j})}[j' \neq j] = 0 \dots \text{otherwise}$

8. Evaluate  $J(u_{i,j+})$

9. Compute the gradient estimate,  $\frac{\delta J}{\delta u_i} \cong \frac{1}{\Delta u_g} [J(u_{i,j+}) - J(u_i)]$

Next actuator  $j$

// Minimize  $J(\tilde{u}(k))$  along the gradient direction given by the affine parameterization  $\tilde{u}(k) = u_i - (k \cdot \Delta u_s \cdot \nabla J(u_i) \cdot \|\nabla J(u_i)\|_2^{-1})$ . Minimize by generating control points over the range  $k = [1..P]$ , generating a piecewise interpolating cubic hermite curve over these points, then minimizing the cubic polynomial representation.

10.  $KJTable.AddPoint(k = 0, J(u_i))$

11. For  $k = [1..P]$

12.  $\tilde{u}(k) = u_i - (k \cdot \Delta u_s \cdot \nabla J(u_i) \cdot \|\nabla J(u_i)\|_2^{-1})$

13. if  $\tilde{u}(k)$  violates the constraints

14. break

15. Evaluate  $J(\tilde{u}(k))$

16.  $KJTable.Add(k, J(\tilde{u}(k)))$

Next  $k$

17.  $(k^*, J^*) = SPLINE\_MINIMIZE(KJTable)$

18.  $u_{i+1} = u(k^*) = u_i - (k^* \cdot \Delta u_s \cdot \nabla J(u_i) \cdot \|\nabla J(u_i)\|_2^{-1})$

// Determine convergence and prepare for next iteration

19.  $\Delta Err\% = 100 \cdot \frac{(J(u_i) - J^*)}{J(u_i)}$

20.  $TotalErr\% = 100 \cdot \frac{(J(u_0) - J^*)}{J(u_0)}$

21. hasConverged =  $(\Delta Err\% < \Delta ErrMin\%)$

End while ! hasConverged

22. Return  $u_{min} = u_{i+1}$

## 2. Fine Optimization Process

The second stage of optimization performs a 'fine optimization' process based on the solution provided by the coarse optimization stage. The fine optimization algorithm is a brute-force descent search.. The variable  $k$  was added to step over plateaus which are created by numerical artifacts in the modeling tool (due to limited accuracy). If the next step would violate a constraint,  $\Delta u$  steps along the constraint surface.

1. Evaluate  $J(u_i)$
2. For each degree of freedom  $j$
3. Find  $k$  and  $J(u_i + k \cdot \Delta u_j)$ 
  - where  $k \geq 1$  is the minimum  $k$  such that  $J(u_i + k \cdot \Delta u_j) \neq J(u_i)$
  - If we are along the constraint, set  $\Delta u_j$  to be along constraint, otherwise let  $\Delta u_j$  varying along each degree of freedom
4. If  $J(u_i + k \cdot \Delta u_j) > J(u_i)$
5.  $u_{i+1} = u_i + k \cdot \Delta u_j$
6. Return to step 1 and advance  $i$
7. else
8. Next  $j$
9. Repeat from step 1 until  $u_{i+1} = u_i$

### 3. Database Caching for Improved Performance

The optimization algorithms above will require extensive and repeat evaluations of the cost function  $J(u)$ . Each iteration requires repeated evaluation in VORLAX over a range of attack angles. To improve performance of the optimizer, a file-based database caching system was created to store all intermediate results that could be quickly accessed (in constant time). The process for evaluating the objective function at a data point is shown in Figure 14.

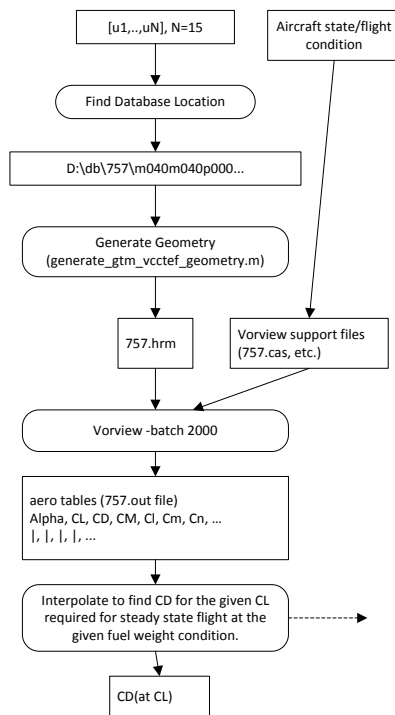


**Figure 14. Evaluation Process with Database Caching.**

## IV. Optimization Results

Optimizations were performed on Linux on a Dell Precision M6400 with a quad-core Intel i7-2760 2.4GHz CPU. A single VORLAX evaluation takes roughly 20-40 seconds. Each evaluation results in 4MB of data. This study required a database of around 100GB in total size. The coarse optimization of one condition averaged around 3 hours to complete; the fine optimization process averaged around 2 hours to complete.

### G. Optimization on Two-Degree-of-Freedom Surface

To test the accuracy of the algorithm, the following test was run allowing only two actuators,  $u_1$  and  $u_2$ , to vary. The results of this initial optimizer test are shown in the following figures, and are summarized in Table 2.

**Table 2. Summary of Results, 2-DOF Optimization Study**

DOF	Relative Angle Constraint	Fuel	# Iterations / # J() Evals	min CD(u,W)	Improvement
2	Inf	80%	4/52	0.009645	2.38%
2	2.0	80%	3/31	0.009662	2.20%
2	1.0	80%	5/44	0.009712	1.68%
2	Inf	50%	5/65	0.009104	1.78%
2	2.0	50%	4/39	0.009111	1.70%
2	1.0	50%	5/47	0.009169	1.06%
2	Inf	20%	4/52	0.008701	4.62%
2	2.0	20%	3/28	0.008749	4.04%
2	1.0	20%	2/17	0.008821	3.20%

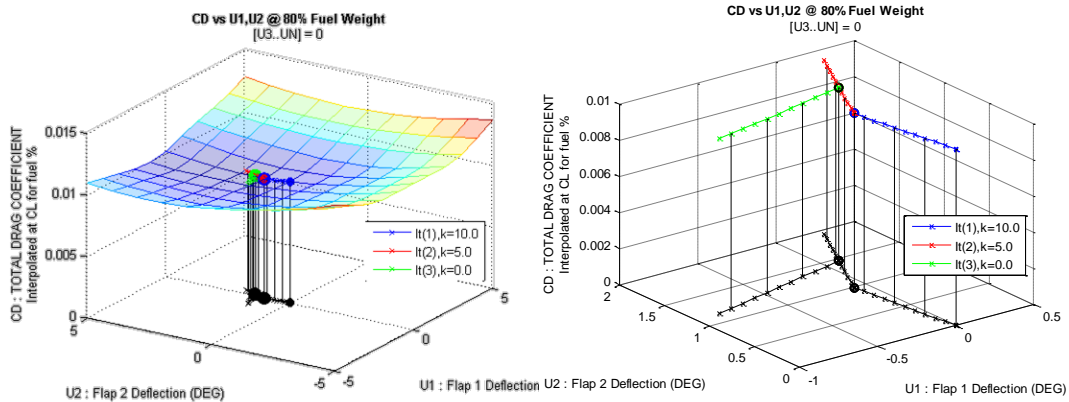


**Figure 15. Unconstrained Optimization over U1-U2.** Optimization progress overlaid on optimization surface (left), optimization trajectory detail (right) at 80% fuel load.

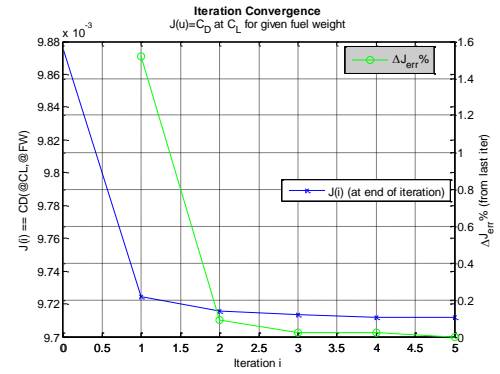
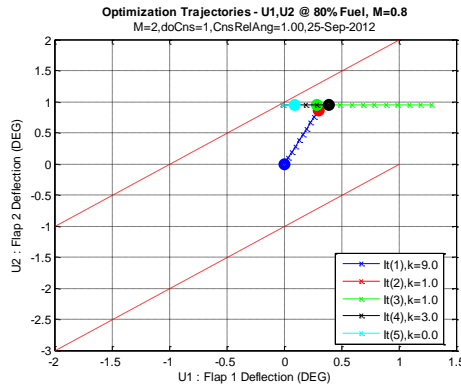
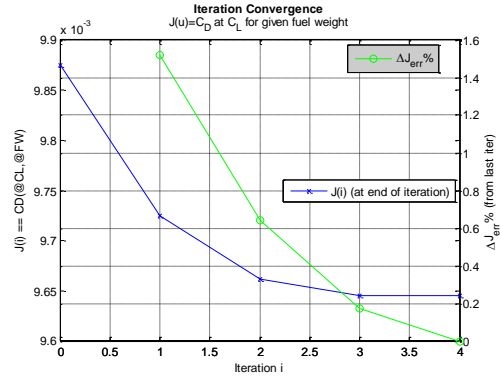
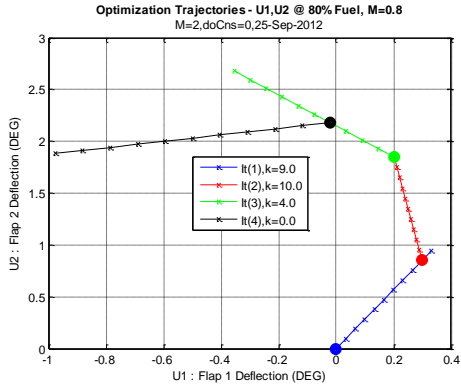


Figure 16. Constrained Optimization over U1-U2, 80% Fuel Load. Unconstrained (top) and 1-degree constraint (bottom).

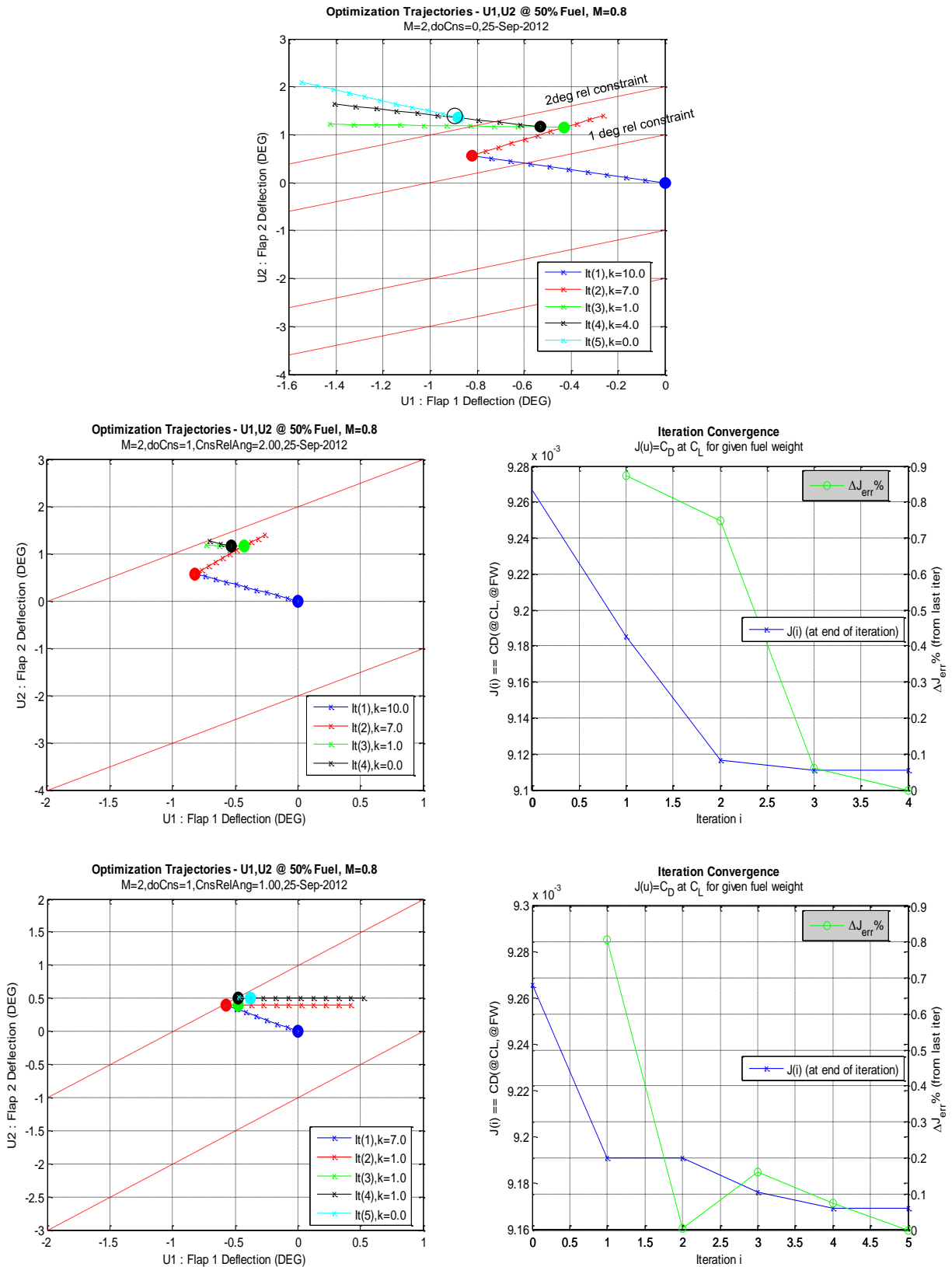


Figure 17. Optimization over U1-U2, 50% Fuel Case.

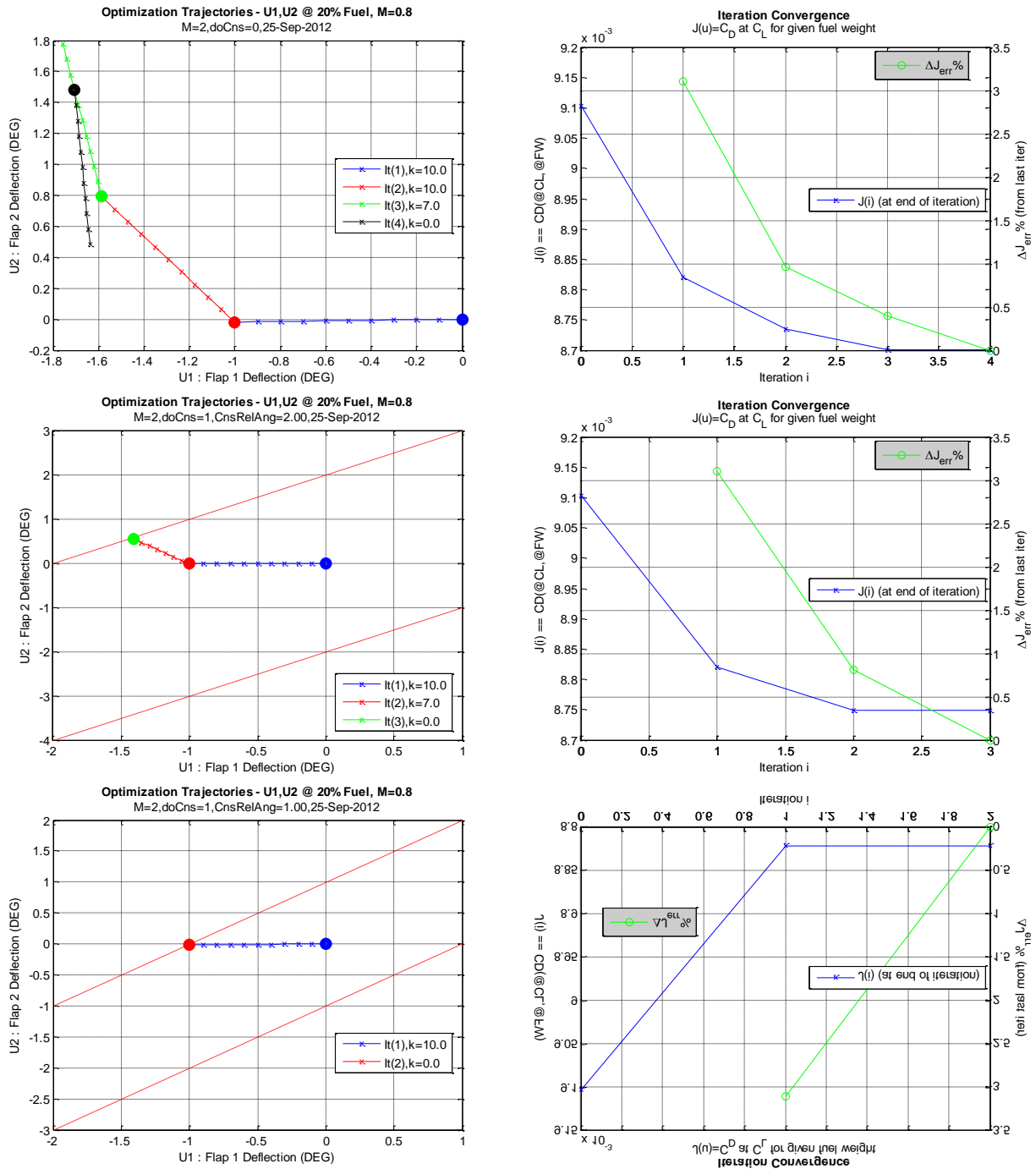


Figure 18. Optimization over U1-U2, 20% Fuel Case.

## H. Optimization Study Over Full VCCTEF System

The optimization engine was used to evaluate the minimum trim drag over VCCTEF input for the 20%, 50%, and 80% fuel load cases. The study allowed the 15 control surfaces to be independently varied and applied symmetrically to the aircraft's left and right wings. The optimization was performed for three relative-angle constraint conditions: unconstrained, 1-degree constraint, and 2-degree constraint. Table 3 summarizes the optimization results. The resulting trajectories are shown in Figure 19, Figure 20, and Figure 21.

**Table 3. Summary of Optimization Results**

<b>DOF</b>	<b>Relative Angle Constraint</b>	<b>Fuel</b>	<b># Iterations / # J() Evals</b>	<b>min CD(u,W)</b>	<b>Improvement</b>
15	Inf	50%	9/234	0.008940	3.64%
15	2	50%	8/193	0.008974	3.26%
15	1	50%	5/106	0.009153	1.23%
15	Inf	80%	4/104	0.009621	2.64%
15	2	80%	4/92	0.009621	2.64%
15	1	80%	4/90	0.009682	1.99%
15	Inf	20%	15/390	0.008326	9.88%
15	2	20%	7/182	0.008611	5.71%
15	1	20%	3/64	0.008818	3.24%

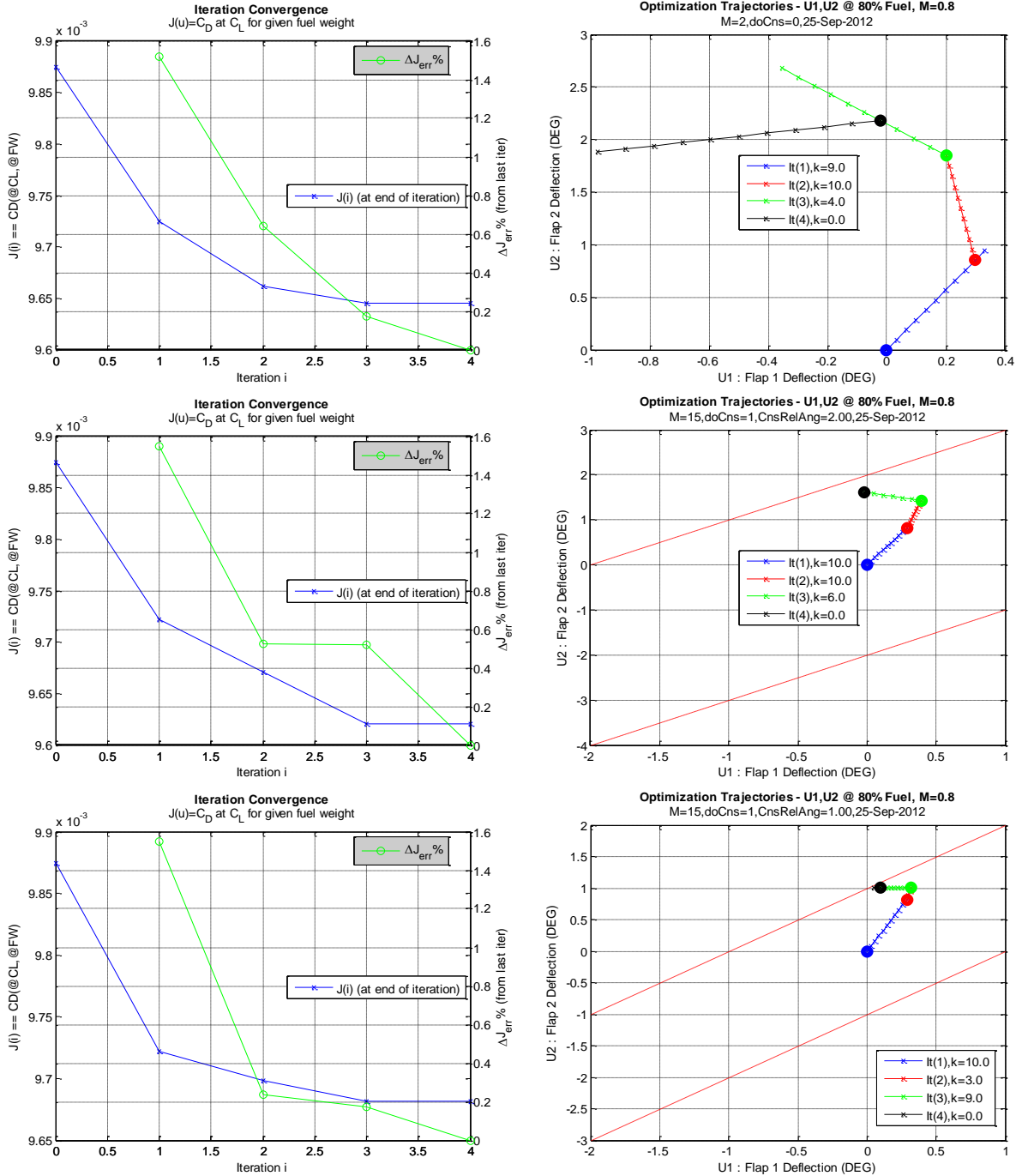
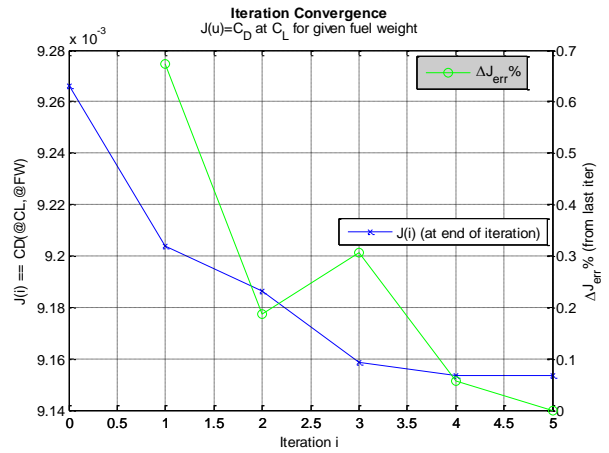
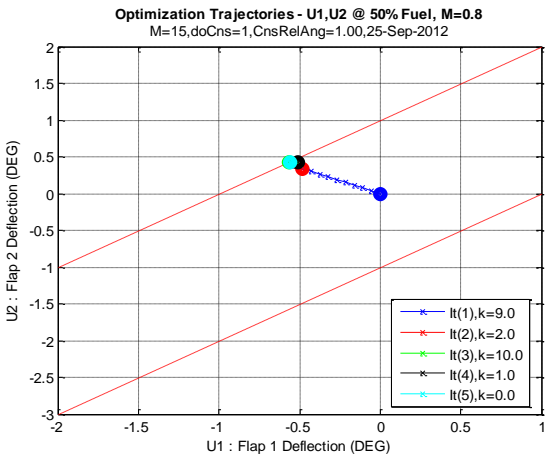
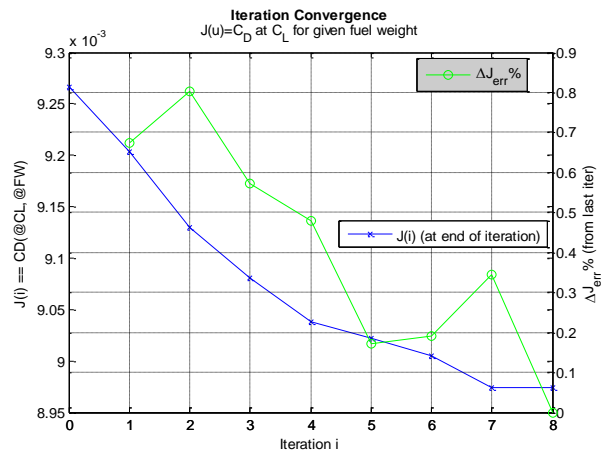
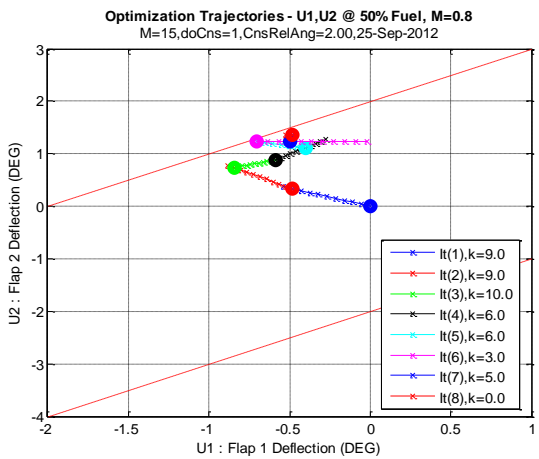
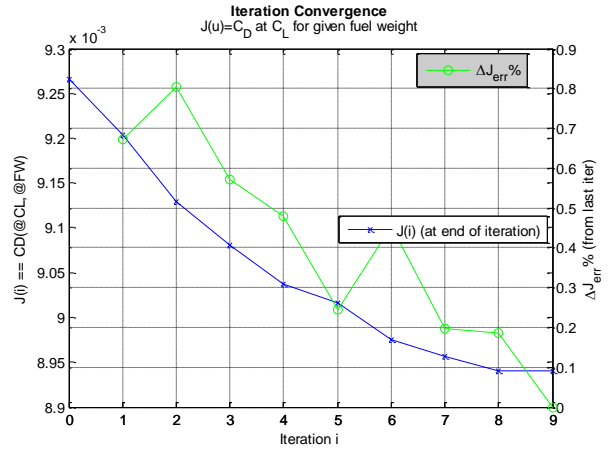
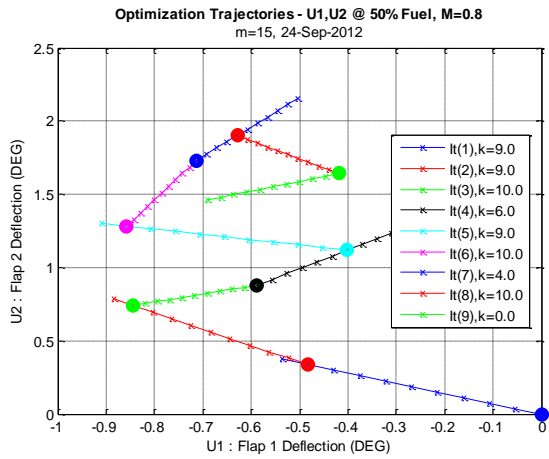
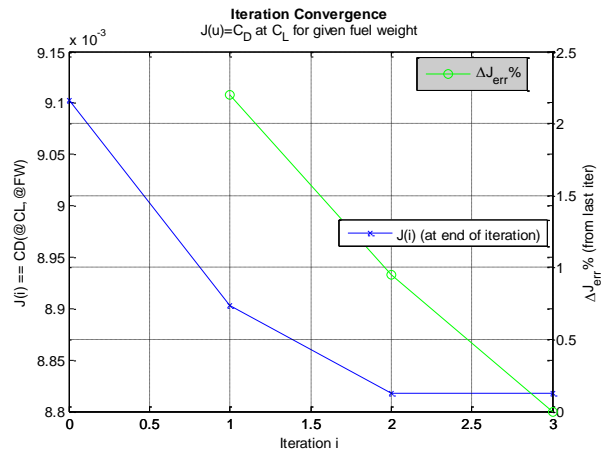
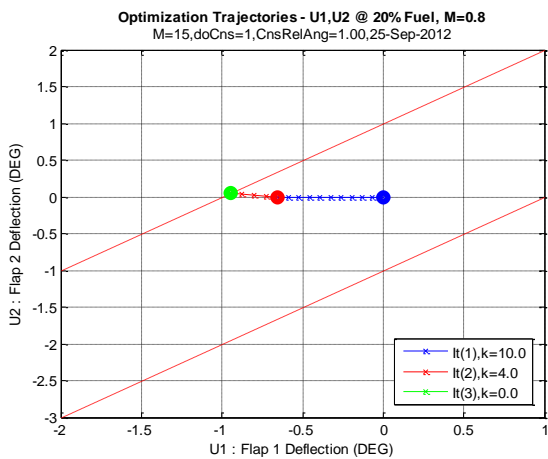
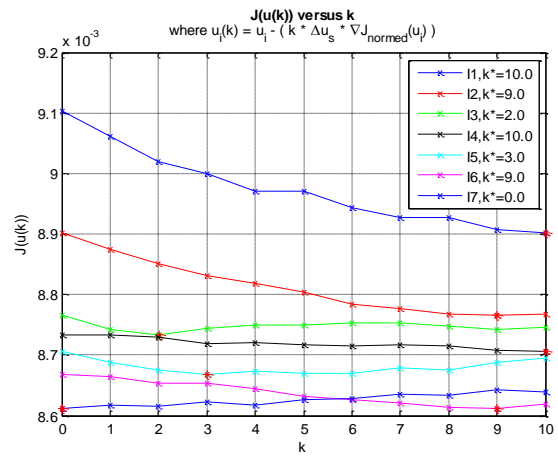
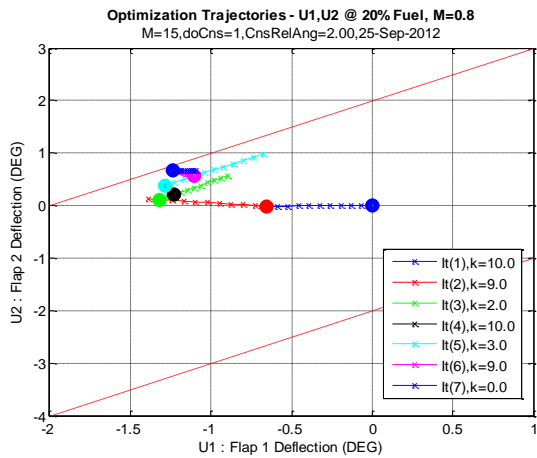
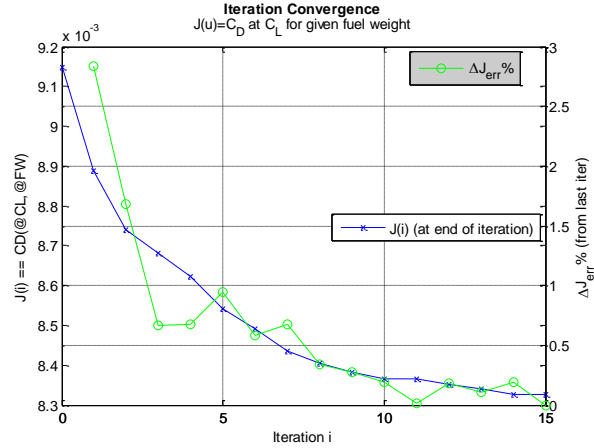
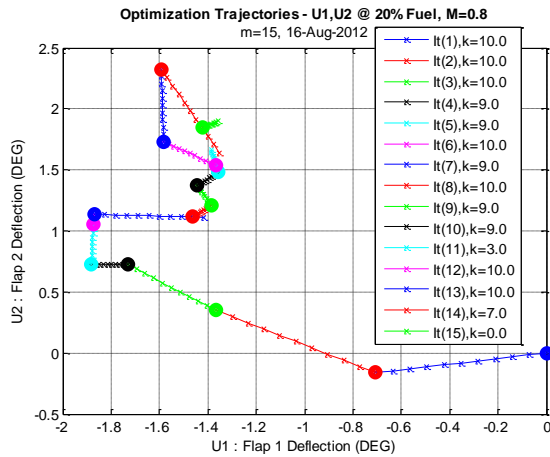


Figure 19. Optimization Results for 80% Fuel Case. Unconstrained (top), 2-degree constraint (middle), 1-degree constraint (bottom).



**Figure 20. Optimization Results for 50% Fuel Case.** *Unconstrained (top), 2-degree constraint (middle), 1-degree constraint (bottom).*



**Figure 21. Optimization Results for 20% Fuel Case. Unconstrained (top), 2-degree constraint (middle), 1-degree constraint (bottom).**

## V. Conclusion

This paper presented the results of an initial assessment of a VCCTEF actuation concept involving 15 distributed control surfaces on the trailing edge of a generic transport-class aircraft in cruise under varying fuel loads. The purpose of this initial assessment was to evaluate the model and generate an initial assessment of drag-saving potential utilizing the VCCTEF. This initial assessment utilizes potential-flow steady-state assumptions in the aerodynamic analysis, and does not include wing flexibility and aeroelastic interaction, which will be the focus of follow-on studies. This paper has presented details of the optimization framework and the modelling tools, which combines a parametric geometry generation tool with vortex-lattice aerodynamic analysis to determine potential trim-drag savings. Performance of the optimizer was improved through a file-based database caching system which stored all intermediate files to speed up repeated evaluations.

This initial study shows promising drag minimization potential of the VCCTEF system, with modest 2.64% drag savings at 80% fuel load, and up to 9.8% for the lightly-loaded aircraft. This study found potential drag savings tend to increase as the aircraft operating weight decreases. The study also analyzed the effect of an elastic material between flap segments. The results suggest that potential drag reduction may be limited by inflexibility of the conformal elastic material between control surface sections.

This initial study forms the basis for optimization of the VCCTEF system. Future studies will expand these results by incorporating aeroelastic effects and wing dynamics into the model. This research provides data for development of real-time control laws that achieve maneuvering objectives while minimizing drag throughout all flight segments of a mission.

## Acknowledgments

The authors wish thank the NASA Aeronautics Research Mission Directorate (ARMD) Fixed Wing Project under the Fundamental Aeronautics Program for support of this research. The authors also wish to acknowledge Mr. John Dykman, Mr. Dan Clingman, Mr. Charles Morris, and Mr. Jim Sheahan from Boeing for technical support in design and aeroelastic model development.

## References

- <sup>1</sup>Nguyen, N., "Elastically Shaped Future Air Vehicle Concept," NASA Innovation Fund Award 2010 Report, October 2010, Submitted to NASA Innovative Partnerships Program, available at [http://ntrs.nasa.gov/archive/nasa/casi.ntrs.nasa.gov/20110023698\\_2011024909.pdf](http://ntrs.nasa.gov/archive/nasa/casi.ntrs.nasa.gov/20110023698_2011024909.pdf).
- <sup>2</sup>Boeing Report No. 2012X0015, "Development of Variable Camber Continuous Trailing Edge Flap System," October 4, 2012.
- <sup>3</sup>Urnes, J., Nguyen, N. and Dykman, J. "Development of a Variable Camber Continuous Trailing Edge Flap System". Fundamental Aeronautics Technical Conference. March 2012.
- <sup>4</sup>Nguyen, N., Urnes, J., "Aeroelastic Modeling of Elastically Shaped Aircraft Concept via Wing Shaping Control for Drag Reduction," AIAA Atmospheric Flight Mechanics Conference, AIAA-2012-4642, August 2012.
- <sup>5</sup>Jordan, T. L., Langford, W. M., Belcastro, C. M., Foster, J. M., Shah, G. H., Howland, G., and Kidd, R., "Development of a Dynamically Scaled Generic Transport Model Testbed for Flight Research Experiments," AUVSI Unmanned Unlimited, Arlington, VA, 2004.
- <sup>6</sup>Miranda, L.R., Elliot, R.D., and Baker, W.M., "A Generalized Vortex Lattice Method for Subsonic and Supersonic Flow Applications," NASA CR-2865, 1977.
- <sup>7</sup>Nguyen, N., Trinh, K., Nguyen, D., Tuzcu, I., "Nonlinear Aeroelasticity of Flexible Wing Structure Coupled with Aircraft Flight Dynamics," AIAA Structures, Structural Dynamics, and Materials Conference, AIAA-2012-1792, April 2012.
- <sup>8</sup>Urnes, J., Nguyen, N., Ippolito, C., Totah, J., Trinh, K., Ting, E. "A Mission-Adaptive Variable Camber Flap Control System to Optimize High Lift and Cruise Lift-to-Drag Ratios of Future N+3 Transport Aircraft," 51st AIAA Aerospace Sciences Meeting including the New Horizons Forum and Aerospace Exposition, AIAA-2013-0214. 2013.
- <sup>9</sup>Somers, D. M. "Effect of Flap Deflection on Section Characteristics of S813 Airfoil," NREL/SR-500-36335, NREL Subcontractor Report, Contract No. DE-AC36-99-GO10337, January 2005.